PROCEEDINGS OF SCIENCE

4U 0115+63: phase lags and cyclotron resonant scattering

Carlo Ferrigno[*,a] **M. Falanga,**[b] **E. Bozzo,**[a] **P. A. Becker,**[c] **D. Klochkov,**[d] **and A. Santangelo**[d]

[a] *ISDC data center for astrophysics, Université de Genève, chemin d'Écogia, 16 1290 Versoix Switzerland*
[b] *International Space Science Institute (ISSI) Hallerstrasse 6, CH-3012 Bern, Switzerland*
[c] *Department of Computational and Data Sciences*
George Mason University
4400 University Drive, MS 6A3 Fairfax, VA 22030
[d] *IAAT, Abt. Astronomie, Universität Tübingen, Sand 1, 72076 Tübingen, Germany*
E-mail: carlo.ferrigno@unige.ch

We study the energy dependent pulse profiles and phase resolved spectra of the high-mass X-ray binary pulsar 4U 0115+63 to investigate the role of cyclotron resonant scattering in the pulse profile formation. For this purpose, we exploit archival *BeppoSAX* and *RXTE* data taken during the bright phase of the giant outburst occurred in 1999.

We find that the pulse profiles are significantly shifted and distorted at the energies corresponding to the cyclotron scattering absorption features. We develop a geometrical model of the column emission and pulse profile formation that explains this newly discovered phenomenon, finding that it can be modeled as an energy dependent angular beaming of the radiation emitted by the column.

Data with higher S/N and more sophisticated theoretical models will contribute significantly to the comprehension of the X-ray emission in the strong gravitational and radiative fields of accreting neutron stars.

Fast X-ray timing and spectroscopy at extreme count rates: Science with the HTRS on the International X-ray Observatory - HTRS2011,
February 7-11, 2011
Champèry, Switzerland

[*] Speaker.

PoS(HTRS 2011)055

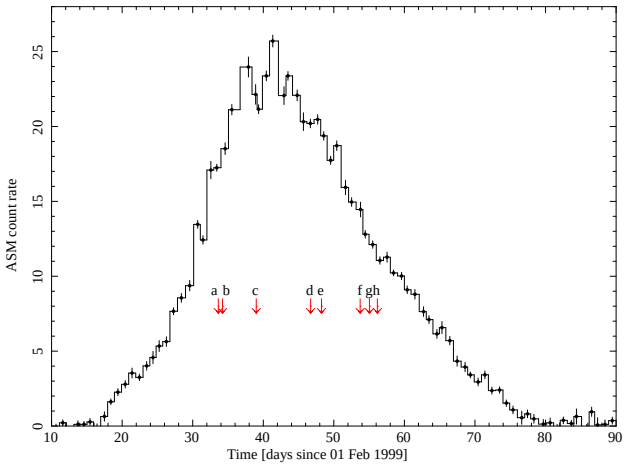

Figure 1: All Sky Monitor light curve in the 2-10 keV energy range. The red arrows indicate the start time of the observations analyzed in this work and their conventional names. Observations (a), (d), and (f) were performed with *BeppoSAX*, the others with *RXTE*.

1. Introduction

4U 0115+63 is an extensively studied accreting neutron star (NS) orbiting around a Be star. This system underwent several giant outbursts since its discovery in 1969 (Whitlock et al. 1989), reaching a luminosity of $\sim 10^{38}$ erg/s. In this contribution, we study the bright phase of the outburst occurred in 1999 when long, uninterrupted observations using *RXTE* and *BeppoSAX* were performed. These observations allowed us to unveil the energy dependency of the pulse profile at energies close to that of the CRSFs[1]. Our conventional naming of the observations is shown in Fig. 1 labeling the red arrows.

The NS has an eccentric orbit ($e = 0.34$) with a period of 24.3 days and it spins on its axis in $\sim$3.6 s. The light curve folded at the spin period, the "pulse profile", exhibits a strong energy and luminosity dependency during the outbursts, with the exception of their bright phase, when it remains approximatively stable (see Fig. 2). The source spectrum can be fitted either with phenomenological functions or with a multi-component physically motivated model, which naturally explains the dramatic change of the pulse profile morphology at low energy (Ferrigno et al. 2009). The soft component can be interpreted as the Comptonization of a $\sim$0.6 keV black-body from a cloud of electrons with optical depth $\tau \sim 24$ and $kT \sim 2.9$ keV. Its contribution to the flux is roughly constant throughout the spin phase. The hard component is due to the Comptonization of cyclotron emission from the collisional excitation of the first Landau level by a hotter plasma residing in the accretion column ($\sim$6 keV, model from Becker & Wolff 2007); it is prominent along the pulse peak. A cyclotron scattering feature at $\sim$11 keV is observed together with 5 higher harmonics (see Heindl et al. 2004; Ferrigno et al. 2009, and references therein).

[1] A comprehensive journal paper has been submitted with all the details of our analysis (Ferrigno et al. 2011).

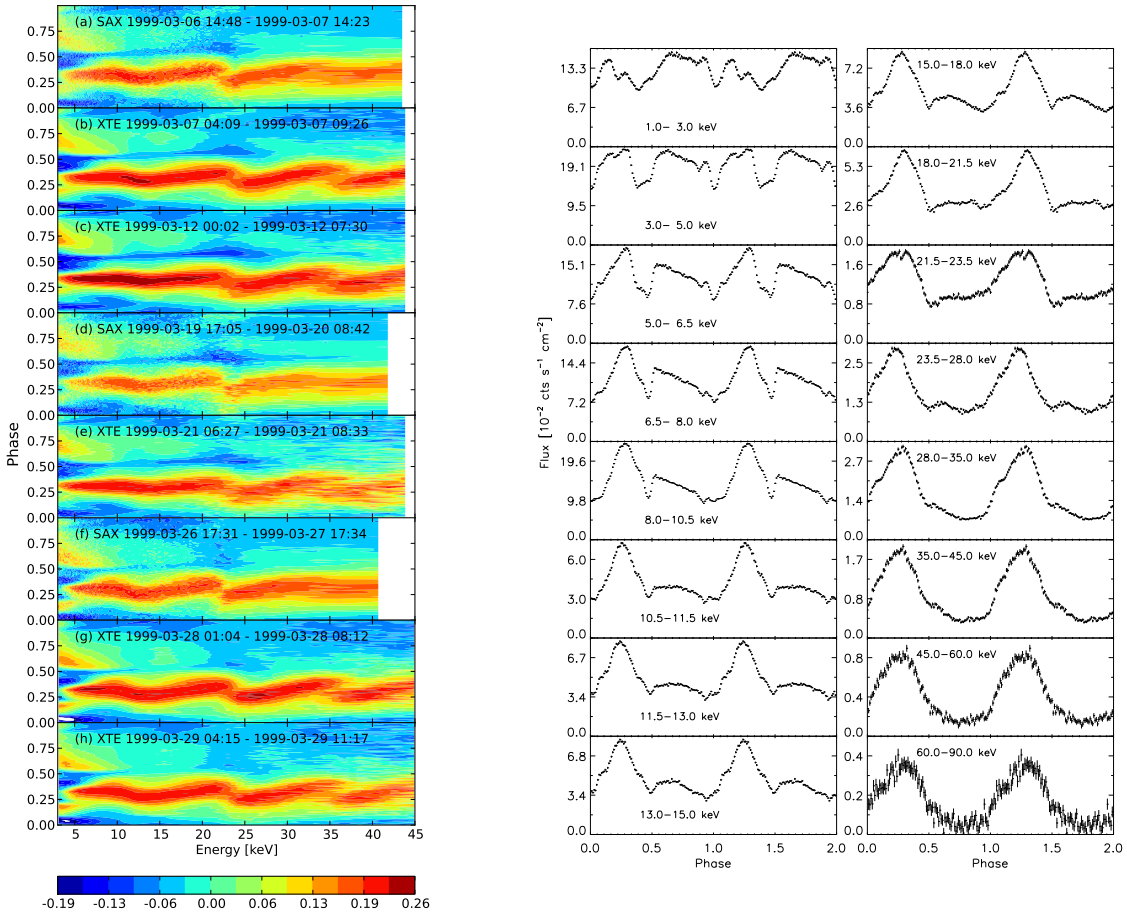

Figure 2: *Left panel*: pulse profiles scaled to have zero average and unitary standard deviation as a function of energy. Red (blue) colors indicate higher (lower) count-rates at different pulse phases and energies. The higher intensity is around phase $\sim$0.3, in correspondence with the "main peak". *Right panel*: pulse profiles during observation (a) in different energy ranges. Data were collected with the *MECS* (2–8.5 keV), the *HPGSPC* (8.5–24 keV) and the *PDS* (24–90 keV) instruments on board of *BeppoSAX*.

2. Results

2.1 Pulse profile analysis

To highlight the varying morphology of the pulse profiles with energy, we extracted pulse profiles in the smallest possible energy bands compatible with the instrumental resolution and a sufficient S/N. We then subtracted the average count rate from each pulse profile and divided it by its standard deviation. A color coded image of the pulse profiles in each observation is shown in Fig 2, left panel.

There is a phase modulation of the pulse peak at energies correspondent to the cyclotron harmonics, to which we refer as "phase lag". To quantify this effect, we perform a correlation analysis: for each observation, we compute the maximum of the cross-correlation function between

each pulse profile and a reference pulse extracted in the 8–10.5 keV energy band as function of phase. We restrict the phase range to the main peak (phase 0.1–0.45 in Fig. 2). A less than unitary correlation in the energy range affected by cyclotron scattering indicates a slightly different shape of the profiles. Errors are computed using Monte-Carlo simulations. To correctly evidence the features visible in the pattern of the phase lags as a function of energy, we fit to these data a model comprising several asymmetric Gaussian lines: the empirical function used to fit the phase lags energy dependency is: $f(e) = A + \sum_{i=1}^{4} N_i \exp\left[-(e-E_i)^2/\sigma^2_{i,\{d,u\}}\right]$, where $\sigma_{i,\{d,u\}} = \sigma_{i,d}$ for $e \leq E_i$, $\sigma_{i,\{d,u\}} = \sigma_{i,u}$ for $e > E_i$, and e is the energy. The fourth Gaussian is only poorly determined due to the low S/N of the data. (Results are represented in Fig. 3).

We note that the intrinsic energy resolutions of the different instruments (not accounted for in our phenomenological fit of the phase lags) affect the estimate of the centroid energies of the Gaussian empirical functions. From Fig. 3 it is clearly visible that the third Gaussian is systematically detected with a centroid energy lower in the *PDS* than in the *PCA* data, as the former instrument is characterized by a lower energy resolution than the latter. The opposite effect is visible on the second Gaussian by comparing the *PCA* with the *HPGSPC* data, as the latter has a finer energy resolution than the former. Taking into account these systematic effects, we conclude that the phase lags measured from the different instruments and observations are in good agreement with each other and no significant variations of the phase lag pattern can be appreciated in the luminosity range of 4U 0115+63 spanned by the data.

2.2 Phase resolved spectroscopy

The source spectrum is known to be phase dependent, in particular the centroid energy of the cyclotron lines. We then investigate the phase dependency of the second harmonic parameters, since it is the most prominent spectral feature and is a good tracer of the magnetic field in the scattering region. Phase resolved spectroscopy confirms a close connection between the phase lags and this cyclotron scattering feature (Fig. 4). It also yields a tight constrain on the stability of the centroid energy in different observations within the investigated luminosity range. Similar results are obtained for the fundamental, while for higher harmonics this kind of analysis is hampered by the poor S/N of the data.

3. A model for the phase lags

To investigate the puzzling origin of these phase shifts, we build a simplified model for the pulse profile formation which accounts for the relativistic ray-tracing effect near a compact object. We assume that the emission originates on the lateral walls of two cylindrical accretion column with an intrinsic beaming depending on the angle formed with respect to the local radial direction (α in Fig. 5). The column aperture and height are tunable parameters, as well as the NS compactness, but are fixed to reasonable values, as they do not influence significantly our findings. With these assumptions, we can compute the asymptotic beam pattern, i.e., the integrated emission of the column as function of the viewing angle indicated as ψ in Fig. 5. This is reported in the central column of Fig. 6. To reconstruct the observed pulse profiles, it is necessary to know the system geometry. The relevant parameter are taken from the pulse decomposition analysis (Sasaki et al.

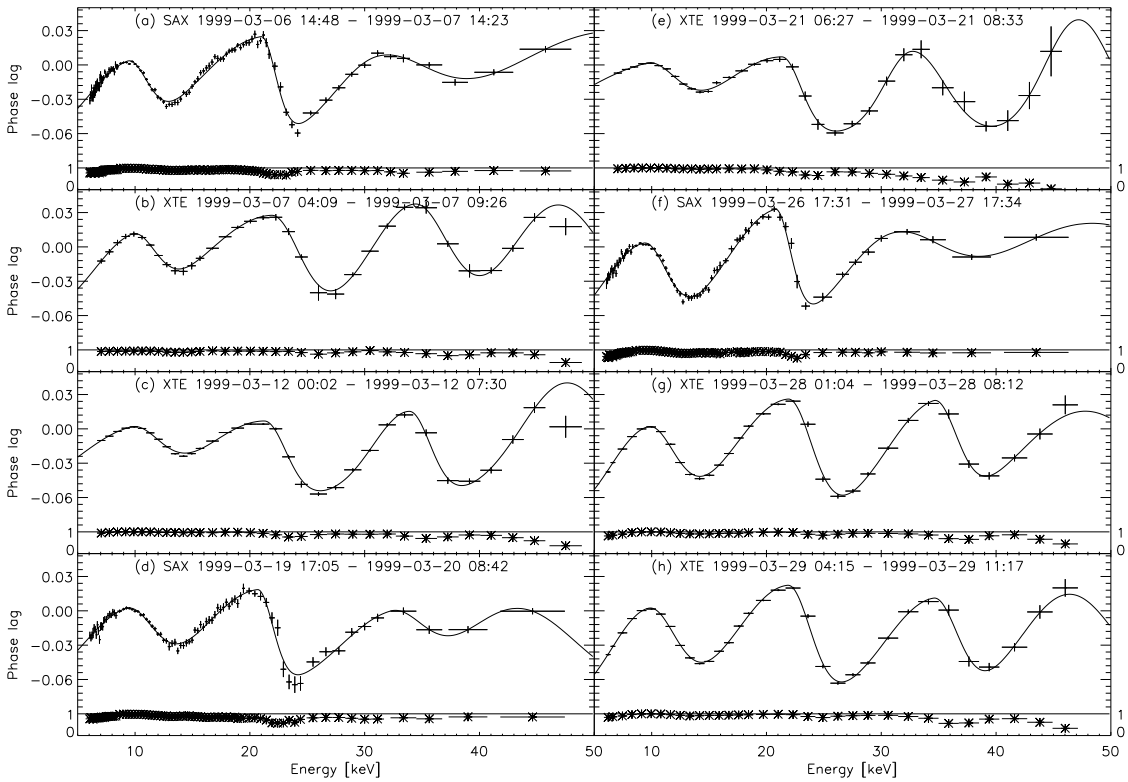

Figure 3: Phase lags of the main peak in normalized phase units (points) and linear correlation coefficients (stars) as a function of energy. The correlation function is computed on a phase interval of 0.4 phase units, centered on the maximum of the reference pulse profiles. The solid line represents the best fit function to the phase lags, made of four asymmetric gaussians plus a constant off-set.

2011) and are: inclination of the rotational axis with respect to the line of sight, $\Theta_0 = 60^o$ (assumed); polar angle of one column with respect to the rotational axis, $\Theta_1 = 74^o$; polar angle of the second column, $\Theta_2 = 148^o$; azimuthal angle of displacement from the antipodal position, $\Delta = 65^o$ (see Fig. 5).

The column intrinsic beaming function is the most controversial issue, since it depends on several factors, such as the velocity and density profiles of the accretion flow, the magnetic field configuration and the specific cross sections of the photon-electron interaction. We adopt an heuristic approach that aims at approximately reproducing the asymptotic column beam pattern reconstructed by Sasaki et al. (2011) with two Gaussian beams: one directed downwards as expected for the relativistically advected radiation produced in the column, one directed upwards to mimic the radiation scattered possibly near the column's base:

$$I_0(\alpha, r) = \sum_{i=1}^{2} N_i \exp\left[-\frac{1}{2}\left(\frac{\alpha - \alpha_i}{\sigma_i}\right)^2\right]. \tag{3.1}$$

In the equation above, $\alpha_1 = 150^o$, $\alpha_2 = 0^o$, $\sigma_1 = 45^o$, $\sigma_2 = 45^o$, $N_1 = 100$ and N_2 assumed values from 0 to 100 to mimic a variable contribution from scattered radiation. We find that a modulation

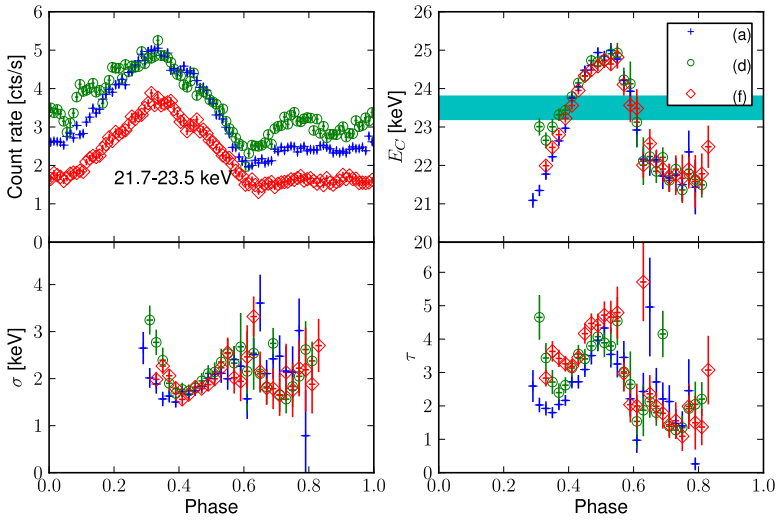

Figure 4: Phase resolved study of the first harmonic for the *BeppoSAX* observations. Blue points correspond to observation (a), green circles to observation (d), and red diamonds to observation (f). Uncertainties on fitted parameters are at 90% c.l. *Upper left*: pulse profiles extracted by using data from the *HPGSPC* in the energy range 21.7-23.5 keV. *Upper right*: centroid energy of the first cyclotron harmonics. The horizontal cyan band is the energy of the maximum phase shift of the main peak measured from the *BeppoSAX* data. *Lower left*: amplitude of the line. *Lower right*: Optical depth of the line.

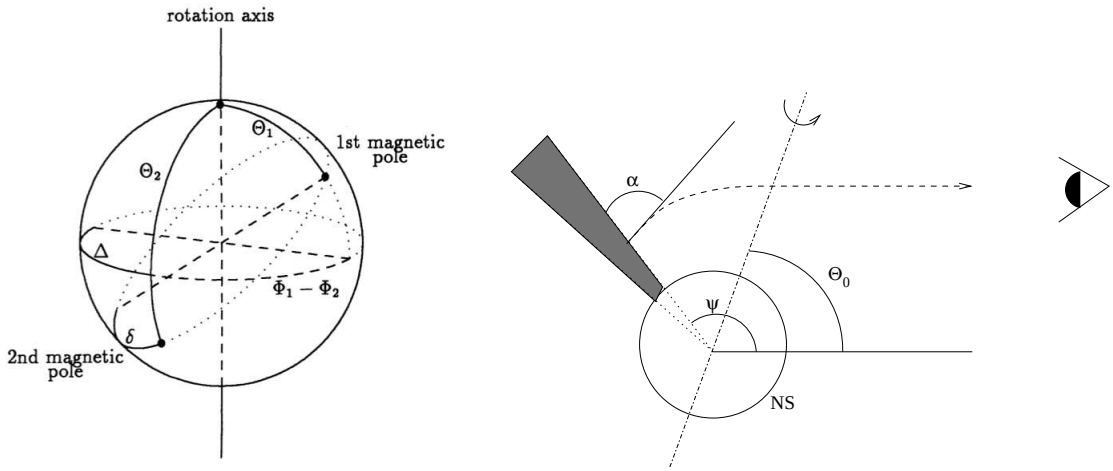

Figure 5: *Left panel*: definition of the system geometry with asymmetric magnetic poles (from Kraus et al. 1995). *Right panel*: the angles relevant for the reconstruction of the column beam pattern. The dashed line is a photon trajectory not in scale.

of the upward radiation can reproduce the observed phase lags of the pulse profiles within the adopted system geometry (see Fig. 6).

A more complex approach, which will solve the radiation transport problem using the actual cross sections and a realistic column velocity profile, shall provide a self consistent model of the spectral and timing characteristics of the XRB X-ray emission. Moreover, significant changes of the pulse profiles with the energy, especially close to the resonances of the cyclotron scattering cross-section, have been reported so far in a number of different XRBPs (e.g., V 0332+53 Tsygankov et al. 2006). The application of the analysis method developed here to these other sources is ongoing.

References

Becker, P. A. & Wolff, M. T. 2007, The Astrophysical Journal, 654, 435

Ferrigno, C., Becker, P. A., Segreto, A., Mineo, T., & Santangelo, A. 2009, Astronomy and Astrophysics, 498, 825

Ferrigno, C., Falanga, M., Bozzo, E., et al. 2011, Astronomy and Astrophysics, submitted

Heindl, W. A., Rothschild, R. E., Coburn, W., et al. 2004, X-RAY TIMING 2003: Rossie and Beyond. AIP Conference Proceedings, 714, 323

Kraus, U., Nollert, H.-P., Ruder, H., & Riffert, H. 1995, Astrophysical Journal v.450, 450, 763

Sasaki, M., Müller, D., Kraus, U., Ferrigno, C., & Santangelo, A. 2011, Astronomy and Astrophysics, submitted

Tsygankov, S. S., Lutovinov, A. A., Churazov, E. M., & Sunyaev, R. A. 2006, Monthly Notices RAS, 371, 19

Whitlock, L., Roussel-Dupre, D., & Priedhorsky, W. 1989, *ApJ*, 338, 381

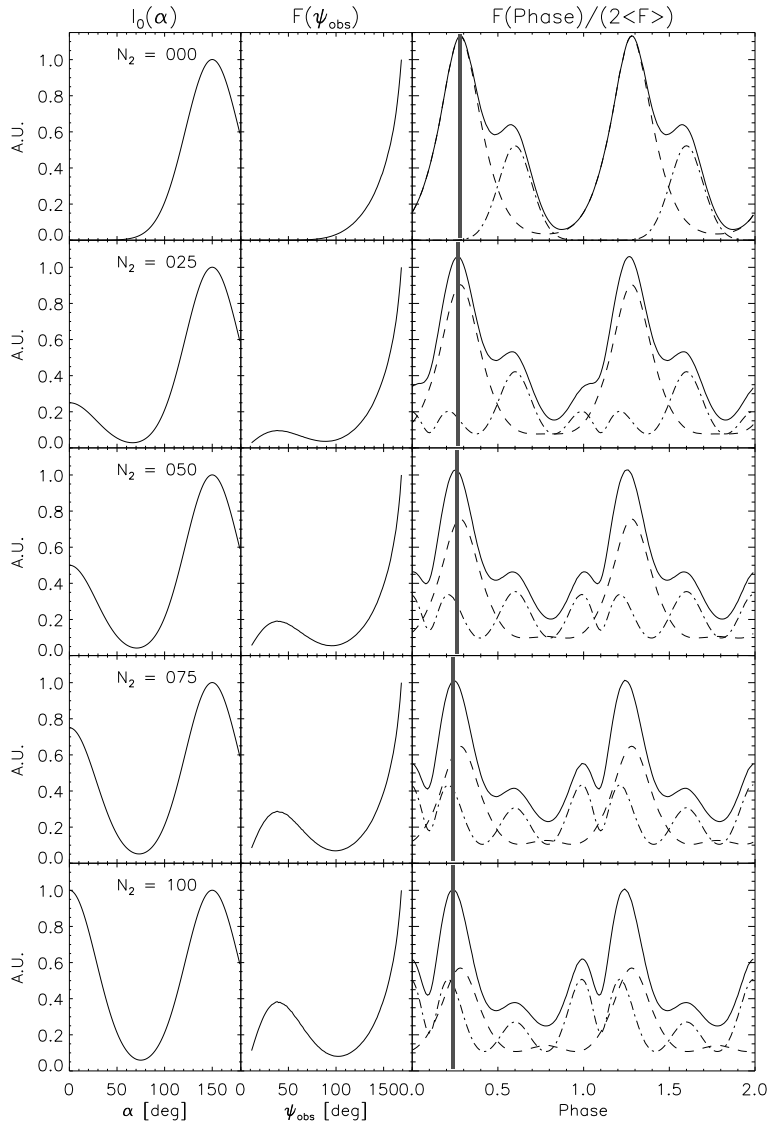

Figure 6: *Left panels*: intrinsic beam patterns (arbitrary units) emerging from the lateral walls of the NS accretion column as a function of the angle α with respect to the local radial direction. The function is the sum of two Gaussians as described in Eq. (3.1). The value of the normalization of the upward Gaussian is indicated in each plot (N_2). *Central panels*: asymptotic beam patterns (arbitrary units normalized to the values at 170 degrees) as a function of the angle $\psi_{\rm obs}$ between the axis of the accretion column and the line of sight to the observer. The beams are computed by assuming an accretion column with a semi-aperture of 4 degrees, and extended for 2 km above the surface of a NS with a mass of $1.4\,M_\odot$ and a radius of 10 km. *Right panels*: synthetic pulse profiles computed for the geometry in 4U 0115+63. The solid line corresponds to the total flux divided by its double averaged value for plotting purposes. The dashed line represents the contribution from the farther pole from the line of sight to the observer, while the dot-dashed line indicates the contribution from the other pole. The gray vertical band corresponds to the location in phase of the pulse maximum. A leftward shift in phase is emerging while increasing the value of N_2, with a maximum lag of ~ 0.04 phase units for $N_2 = 100$.